Earth Surf. Dynam. Discuss., https://doi.org/10.5194/esurf-2018-64
Manuscript under review for journal Earth Surf. Dynam.
Discussion started: 3 September 2018
© Author(s) 2018. CC BY 4.0 License.

Theoretical Interpretation of the Exceptional Sediment Transport of Fine-grained Dispersal Systems Associated with Bedform Categories

Tian Zhao[1], Qian Yu[1], Yunwei Wang[2], and Shu Gao[3]

[1]Ministry of Education Key Laboratory of Coast and Island Development, Nanjing University, Nanjing 210023, China.

[2]College of Harbour, Coastal and Offshore Engineering, Hohai University, Nanjing 210098, China.

[3]State Key Laboratory of Estuarine and Coastal Research, East China Normal University, Shanghai 200062, China.

Correspondence to: Qian Yu (qianyu.nju@gmail.com)

Abstract. Being a widespread source-to-sink sedimentary environment, the fine-grained dispersal system (FGDS) features remarkably high sediment flux, interacting closely with local morphology and ecosystem. Such exceptional transport is believed to be associated with changes in bedform geometry, which further demands theoretical interpretation. Using van Rijn (2007a) bed roughness predictor, we set up a simple numerical model to calculate sediment transport, classify sediment transport behaviors into dune and (mega-)ripple dominant regimes, and discuss the causes of the sediment transport regime shift linked with bedform categories. Both regimes show internally consistent transport behaviors, and the latter, associated with FGDSs, exhibits considerably higher sediment transport rate than the previous. Between lies the coexistence zone, the sediment transport regime shift accompanied by degeneration of dune roughness, which can considerably reinforce sediment transport and is further highlighted under greater water depth. This study can be applied to modeling of sediment transport and morphodynamics.

1 Introduction

Shaped by fine-grained (median grain size d = 15 ~ 150 μm, i.e. 6.0 ~ 2.7 φ) bed, the fine-grained dispersal system (FGDS) is a type of sedimentary environment that is rooted in coastal, riverine, deltaic, marine, and subglacial systems, as well as characterized by remarkably high total sediment fluxes (Ma et al., 2017). In science and engineering disciplines, FGDSs are of great importance because they are crucial source-to-sink systems, highlighting the unique role that suspended sediment transport processes play in developing phenomenal sediment transport. Generated from erosion in sources (mountains and riverbeds), transported as suspended load, and eventually preserved at sinks (coastal zone, continental shelves, and deep seas) (Kuehl et al., 2016; Leithold et al., 2016), riverine fine sediments increase turbidity of estuarine and nearshore waters, forming mud depositional systems of considerable thickness (Gao & Collins, 2014; Wright, 1995). The source-to-sink processes these sediments undergo not only notably alter local sediment dynamic environments (Wright & Nittrouer, 1995), material cycling processes (Blair & Aller, 2012; Kuehl et al., 2016), and ecosystems (Venkatesan et al., 2010), but will shape a distinctive sedimentary system over a long

Earth Surf. Dynam. Discuss., https://doi.org/10.5194/esurf-2018-64
Manuscript under review for journal Earth Surf. Dynam.
Discussion started: 3 September 2018
© Author(s) 2018. CC BY 4.0 License.

time span as well (Gao & Collins, 2014). In addition, knowledge of FGDS will be of great benefit to tackling real-time engineering issues, including navigation channel dredging (van Maren et al., 2015), harbor construction (Winterwerp, 2005), monitoring morphological responses of tidal flat reclamation (Lee et al., 1999; Wang et al., 2012), and predicting coastline changes (Mangor et al., 2017).

Over the past century, established works of sediment transport (e.g. Engelund & Hansen, 1967; Julien, 2010; Soulsby, 1997; van Rijn, 1993) has illustrated total sediment transport from a general perspective including both coarse and fine components. However, recently Ma et al. (2017) reports exceptionally higher sediment transport rate in Huanghe (also known as Yellow River; a FGDS) linked with its fine bed than that in coarse bedded flumes (Guy et al., 1966).

Starting from the Engelund-Hansen sediment transport formula (Engelund & Hansen, 1967) founded on the same flume data set, Ma et al. (2017) derive a generalized Englund-Hansen (GEH) formula of suspended sediment transport based on energy conservation theory, excluding the wash load, the fraction of suspended load that almost does not communicates with local bed and flow (Chien & Wan, 1999):

$$C_{\mathrm{D}} q_s^* = \alpha \theta_{\mathrm{b}}^{\mathrm{n}} \tag{1}$$

where C_{D} is the total bed drag coefficient; $q_s^* = \frac{q_{\mathrm{s}}}{\rho_{\mathrm{s}}\sqrt{(s-1)gd^3}}$ is the dimensionless sediment transport rate, i.e. Einstein number; $q_{\mathrm{s}} = S_* uh$ is the suspended sediment transport rate by mass, and S_* is the vertically averaged suspended sediment concentration (SSC); $\theta_{\mathrm{b}} = \frac{\tau_{\mathrm{b}}}{(\rho_{\mathrm{s}}-\rho)gd}$ is the dimensionless total bed shear stress, i.e. Shields (1936) number; $\tau_{\mathrm{b}} = \rho C_{\mathrm{D}} u^2$ is the total bed shear stress; α is the coefficient of θ_{b}, and n is the exponent of θ_{b}; $s = \rho_{\mathrm{s}}/\rho$ is the specific gravity of sediment grains; g is the gravitational acceleration; c is the total sediment concentration by mass.

By linking Huanghe and the flume data with the GEH formula, Ma et al. (2017) find similar α and n values for distinct zones of d (for Huanghe data, d < 130 μm, α = 0.895, n = 1.678; for the flume data, d > 190 μm, α = 0.0355, n = 3.0); these zones containing data points representing similar sediment transport behaviors (α and n values) can be identified as sediment transport regimes. In between lies a narrow transition zone, where exceptionally high sediment load is initiated as d becomes finer. Furthermore, they suggest that such phenomenal sediment transport is associated with the absence of dune by relating sediment transport regimes to bathymetry data of lower Huanghe (d = 90 μm, low bedform height) and lower Mississippi River (d = 280 μm, significant dune presence).

Notwithstanding these recent advances, a quantitative theoretical interpretation of the relationship between sediment transport regimes and prevailing bedforms is still absent, yet achievable through parameterizing the relationship between bedform geometry and sediment transport rate. Unlike preceding semi-empirical ways, we try to interpret the mentioned problems with sediment dynamic theories that bridge the gap between bedform prediction and sediment transport modeling. In this paper, we first set up a sediment transport model based upon van Rijn (2007a) bedform roughness predictor, then analyze the model calculation results to classify sediment transport behaviors into two regimes and a transition zone, and finally discuss the causes of the regime shift in sediment transport associated with bedform changes.

© Author(s) 2018. CC BY 4.0 License.

2 Methods

2.1 Theories

In order to estimate the sediment transport in FGDSs associated with bedform changes, a numerical model is set up to calculate values of variables in the GEH formula, so as to explore the relationship between the suspended sediment transport rate q_s, a proper approximation of total sediment flux when $d < 250$ μm (van Rijn, 2007a), and dimensionless total bed shear stress θ_b.

The suspended sediment transport rate $q_s = S_* uh$ is controlled by depth-averaged flow speed u and SSC S_*, which is particularly governed by their vertical profiles. Based on the basic assumptions that (1) currents are the sole driving force of sediment transport, (2) flows over the bed are unstratified, and (3) suspended sediment transport dominates total sediment transport when $d < 250$ μm, the logarithmic law of the wall:

$$U(z) = \frac{u_*}{\kappa}\ln(\frac{z}{z_0}) \tag{2}$$

and the Rouse (1937) profile:

$$\begin{cases} c(z) = c_\mathrm{a}\left(\frac{z}{z_\mathrm{a}}\frac{h-z_\mathrm{a}}{h-z}\right)^{-b} \\ b = \frac{w_s}{\kappa u_*} \end{cases} \tag{3}$$

are utilized in this model to derive u and S_*, directing to the final estimate of total sediment transport rate.

In the law of the wall, $U(z)$ stands for the horizontal flow speed at height z to the bed, $u_* = \sqrt{\tau_\mathrm{b}/\rho} = \sqrt{C_\mathrm{D}} \cdot u$ is the friction velocity, $\kappa = 0.4$ denotes the von Kármán constant, and z_0 refers to the total roughness length. In the Rouse profile, $c(z)$ symbolizes the suspended sediment concentration at height z to the bed, c_a signifies the reference concentration (i.e. the SSC at reference height z_a) by mass; b represents the Rouse number, which is decided by u_* and w_s, the settling velocity of bed sediment.

Being the average of $U(z)$, u is linked to C_D (related to u_* and z_0) and τ_b (related to u_*). Similarly, S_* is associated with the ripple roughness height $k_{s,r}$ (related to z_a), d (related to c_a and w_s), C_D (related to u_*), τ_b (related to u_*), and skin bed shear stress $\tau_\mathrm{bs} = \rho C_\mathrm{Ds} u^2$ (related to c_a). Given vertically averaged flow speed u, median bed grain size d, and water depth h, we still need to figure out total bed drag coefficient C_D, skin bed drag coefficient C_{Ds}, and ripple roughness height $k_{s,r}$ to finish the calculation of sediment transport rate.

C_D is a function of total bed roughness height $k_s = 30\, z_0$ and water depth h (Soulsby, 1997):

$$C_\mathrm{D} = \left[\frac{\kappa}{1+\ln\left(\frac{z_0}{h}\right)}\right]^2 = \left[\frac{\kappa}{1+\ln\left(\frac{k_\mathrm{s}}{30h}\right)}\right]^2 \tag{4}$$

Likewise, C_{Ds} is a function of grain roughness height $k_{s,g} = 2.5\, d$ (Nikuradse, 1933) and water depth h (Soulsby, 1997):

$$C_\mathrm{Ds} = \left[\frac{\kappa}{1+\ln\left(\frac{k_\mathrm{s,g}}{30h}\right)}\right]^2 = \left[\frac{\kappa}{1+\ln\left(\frac{d}{12h}\right)}\right]^2 \tag{5}$$

Earth Surf. Dynam. Discuss., https://doi.org/10.5194/esurf-2018-64
Manuscript under review for journal Earth Surf. Dynam.
Discussion started: 3 September 2018
© Author(s) 2018. CC BY 4.0 License.

Earth Surface Dynamics Discussions Open Access EGU

$k_{s,g}$ and k_s symbolize bed friction from different perspectives. The grain roughness $k_{s,g} = 2.5d$ is only related to the grain size of bed sediments, referring to skin friction on the bed, whereas the total bed roughness height k_s is estimated in relation to bedform size, a function of the mobility parameter $\Psi = \frac{u^2}{(s-1)gd}$ (Manohar, 1955) and water depth h (van Rijn, 2007a).

k_s is composed of three components, namely ripple roughness height $k_{s,r}$, megaripple roughness height $k_{s,mr}$, and dune roughness height $k_{s,d}$ (van Rijn, 2007a). In this study, as the mobility parameter Ψ increases, $k_{s,r}$ was linearly weakened from 150d to 20d, while both $k_{s,mr}$ and $k_{s,d}$ first grow from zero and then decrease. Subsequently, when Ψ is very large (over 600), $k_{s,mr}$ remains 0.02f_{fs} (f_{fs} denotes fine sand factor. For $d \geq 100$ μm, $f_{fs} = 1$; for $d < 100$ μm, $f_{fs} = 10000d$), a value usually larger than $k_{s,r}$ by an order of magnitude, whereas $k_{s,d}$ is cleared. In this regard, $k_{s,d}$ is normally predominant in k_s when Ψ is small, but no longer exists when $\Psi \geq 600$.

In addition, $k_{s,g}$ and k_s interact with the flow in different ways. Determined by $k_{s,g}$, the skin portion of bed shear stress $\tau_{\mathrm{bs}} = \rho C_{\mathrm{Ds}} u^2$ directly initiates sediment movement and suspension. Meanwhile, with a considerable input from form drag, k_s decides the total bed drag coefficient C_D, which (1) significantly increases total bed shear stress $\tau_{\mathrm{b}} = \rho C_{\mathrm{D}} u^2 = \rho u_*^2$ by directing its majority to balancing bedform drag, and (2) motivates vertical distribution of turbulence, which resists vertical stratification and diminishes the Rouse number b. In this regard, changes in the mobility parameter Ψ lead to different bedforms, which furthermore affect sediment transport rates.

For simplicity, our detailed algorithm is listed in Supporting Information S1 for readers' reference.

2.2 Model settings

For current-induced sediment transport in FGDSs, van Rijn (2007a) summarizes that q_s, the transport rate of suspended load, is larger by one order of magnitude than q_b, the transport rate of bedload, as long as the grain size d of bed sediment does not exceed 250 μm (2.0 φ). To underscore the role suspended sediment transport plays in FGDSs, we set the upper boundary of bed sediment grain size d as 250 μm (2.0 φ), so that q_s will remain a good approximation of the total sediment flux. As a non-cohesive modeling approach, the lower boundary of d here is placed at 62.5 μm (4.0 φ), the tipping point between sand and silt. Thus, in this numerical study, the grain size of bed sediment, d, ranges from 4.0 φ to 2.0 φ, with step length 0.1 φ.

In the same time, covering scenarios in real-time fluvial and coastal settings, the water depth h is continuously doubled from 0.3125 m to 20 m, and the vertically averaged horizontal flow speed u is increased from 0.5 m/s to 1.5 m/s at a 0.1 m/s step size.

3 Results

With the above settings, we calculate ripple roughness height $k_{s,r}$, megaripple roughness height $k_{s,mr}$, dune roughness height $k_{s,d}$, total bed roughness height k_s, total bed drag coefficient C_D, dimensionless total bed shear stress θ_b, and

© Author(s) 2018. CC BY 4.0 License.

dimensionless sediment transport rate q_s^* for each case that combines specific median grain size *d*, water depth *h*, and flow speed *u*. These calculation results are saved in Data Set S1.

To highlight the importance of regime shift in sediment transport, we present a log-log plot, featuring the relationship between $C_D q_s^*$ (y-axis), the product of total bed drag coefficient C_D and dimensionless sediment transport rate q_s^*, and the dimensionless total bed shear stress θ_b.

In Figure 1, data points on the same straight line share identical exponent *n* and coefficient *α* of dimensionless bed shear stress θ_b in the GEH formula ($C_D q_s^* = \alpha \theta_b^n$), thus belong to a specific sediment transport regime. Based on this conclusion, data points are therefore categorized into dune dominant and (mega-)ripple dominant sediment transport regimes, according to their different transport behavior (as marked in ovals in each graph) and their predominant component of k_s (see Data Set S1); typical sediment transport behavior in FGDSs corresponds with the (mega-)ripple dominant regime (pink ovals).*α* and *n* are subsequently calculated for both dune and (mega-)ripple dominant regimes in each case; they are listed in Data Set S1 as well. Sandwiched by these two regimes is the narrow coexistence zone, where sediment transport behavior is influenced by both regimes (Lapotre et al., 2017) and undergoes notable changes.

4 Discussion

4.1 The predominant bedform category of a sediment transport regime

As van Rijn (2007a) and our calculation suggest, we set $\Psi = 400$ and $\Psi = 600$ as criteria for defining bedform categories (Figure 2). In the dune region ($\Psi < 400$), the dune roughness height $k_{s,d}$ is predominant in the total bed roughness height k_s, whereas $k_{s,d}$ diminishes rapidly in the transition zone ($400 \leq \Psi < 600$) and ultimately stays zero in the (mega-)ripple region ($\Psi \geq 600$) (Figure 3); the megaripple roughness height $k_{s,mr}$ takes control of k_s then.

Based on the classification of bedform categories, we further propose related cut-off points for sediment transport regimes. For typical flow speed values ($u \in [0.5, 1.5]$ (m/s)) in fluvial and coastal environments, if a particular bedform category prevails (the contribution of such bedform data points counts for more than 50% on a grain-size-fixed bed), then the corresponding sediment transport regime is referred to this type of bedform. Hence, $d = 3.22$ φ and $d = 2.63$ φ are identified as tipping points of sediment transport regimes (Figure 2).

Chien et al. (1987) took Yellow River (Huanghe) as an example and notice that, in FGDSs, bedform drag can be far greater than the skin part of total bed friction in lower flow regime, and will diminish considerably to almost zero in upper flow regime. As suggested above, sediment transport regimes are closely associated with the predominant bedform category. In the dune region ($\Psi < 400$, i.e. lower flow regime or coarse bed), $k_{s,d}$ upholds a considerable weight (usually more than 50%, Figure 3) in k_s, leading to a larger total bed drag coefficient C_D and dissipating the majority of total bed shear stress τ_b to overcoming significant dune friction; only a small fraction of total bed shear stress is utilized for suspended sediment transport. However, in the (mega-)ripple region ($\Psi \geq 600$, i.e. upper flow

© Author(s) 2018. CC BY 4.0 License.

regime or fine bed, the representative setting in FGDSs), dunes are destroyed ($k_{s,d}$ = 0, Figure 3) by the flow over bed, which can reduce the total k_s by up to one order of magnitude and halve the total C_D (see Data Set S1). In the meantime, the importance of grain roughness $k_{s,g}$ has increased, initiating the exceptional suspended sediment transport (Figure 1). Therefore, we suggest that increased Ψ (stronger fluid flow or finer bed sediment) accelerates the degeneration of dunes and the considerable decline in C_D, greatly enhancing suspended sediment transport, finally shaping the two disparate sediment transport regimes (dune dominant and (mega-)ripple dominant).

4.2 Comparison with measured data: Importance of water depth

Derived from field survey results in the Yellow River (Huanghe, $h \approx 0.55 \sim 7.8$ m) and findings of Guy et al. (1966)'s (GSR) flume experiments ($h \approx 0.06 \sim 0.40$ m), Ma et al. (2017) present Logistic curves, underlining sediment transport regime shifts, i.e. changes in exponent n and coefficient α of dimensionless bed shear stress θ_{b} in the GEH formula ($C_{\mathrm{D}} q_{\mathrm{s}}^* = \alpha\theta_{\mathrm{b}}^{\mathrm{n}}$), with respect to bed sediment grain size d. Both n and α are indicators of bedform geometry (Engelund & Hansen, 1967). In comparison with their results, our numerical experiments (h = 0.625 ~ 10 m) illustrate similar trends in sediment transport regimes, regime shifts (coexistence zone), and estimated n and α (Figure 4).

In our (mega-)ripple dominant regime of sediment transport (d = 3.22 ~ 4.0 φ), equivalent to their zone of suspended sediment domination (Huanghe data, with d finer than 2.94 φ), our calculated mean n and α are (2.3 ~ 2.8) and (0.10 ~ 0.76) respectively, while theirs are 1.678 and 0.895 correspondingly. As for our dune dominant sediment transport regime (d = 2.0 ~ 2.63 φ), comparable to their sector of suspended load and bedload coexistence (GSR flume data, with d coarser than 2.40 φ), our estimated mean n and α are (3.5 ~ 4.6) and (0.028 ~ 0.033) correspondingly, whereas theirs are 3.0 and 0.0355 respectively. Both approaches suggest that for finer bed sediments, the exponent n is smaller, but the coefficient α is larger; finer beds advocate remarkable efficiency and flux of suspended sediment transport. In view of the regime shift in sediment transport behavior, our results demonstrate a coexistence band with d = (2.63 ~ 3.22) φ, while they show a transition zone in d = (2.40 ~ 2.94) φ.

Molinas & Wu (2001) point out the importance of water depth h in the original Engelund-Hansen (EH) formula. Derived out of Guy et al. (1966)'s flume experiment data, the original EH formula is only compliant with small water depths (h < 0.5 m) and should be tested and even revised for larger h, due to differences in bedform development for small and large h. By grouping different typical d, u, and h values in FGDSs in our calculation, we compensate for the lack of typical scenarios with different water depths in previous studies of FGDSs and furthermore demonstrate a diverging trend in data points for increasing water depths.

Given small water depths (e.g. h < 1 m), dune ($k_{s,d}$) and megaripple ($k_{s,mr}$) components of total bed roughness height k_s are comparable (Figure 3 & Data Set S1), regardless of the grain size d of bed sediment. Thus, although data points within a certain prevailing bedform (dune or (mega-)ripple) can indicate similar sediment transport behavior, it is not easy to tell apart different sediment transport regimes merely according to their data plots (Figure 1); the corresponding regime shift as reflected by n and α (Figure 4) is not obvious as well. But in view of rising h, as the dune roughness height $k_{s,d}$ becomes prevailing in the total bed roughness height k_s (Figure 3), dune dominant and (mega-)ripple

Earth Surf. Dynam. Discuss., https://doi.org/10.5194/esurf-2018-64
Manuscript under review for journal Earth Surf. Dynam.
Discussion started: 3 September 2018
© Author(s) 2018. CC BY 4.0 License.

dominant sediment transport regimes commence to diverge (Figure 1, Figure 4), and the regime shift indicated by n and α (Figure 4) is thus more apparent.

Limited by room height, the water depth of flume experiments is usually on the order of ($10^{-1} \sim 10^{0}$) m (Guy et al, 1966), whereas fluvial (Ma et al, 2017) and coastal systems (Gao & Collins, 2014) feature a typical water depth on the order of ($10^{0} \sim 10^{2}$) m. As shown in van Rijn (2007a)'s formulae and our discussion above, the extent of bedform development and, consequently, the suspended sediment transport behavior are strongly influenced by water depth, in addition suggesting that a measured data set is comparable to another only if their water depths share the same order of magnitude. Hence, it is of great necessity to take water depth h into consideration in future studies of suspended sediment transport in FGDSs by distinguishing bedforms in small and large water depths.

4.3 Future work

Our study is a preliminary numerical attempt to examine the unique sediment transport behavior of FGDSs. In reality, due to FGDSs' high SSC, vertical stratification is amplified to a considerable extent under small u (Baas et al., 2009); even C_D is not vertically uniform, and the logarithmic law of the wall and Rouse profile will then no longer applicable for the whole water column. Under this circumstance, the water column should be sliced into layers in which vertical stratification is insignificant, and a revised (Rodi & Mansour, 1993) second-order k-ε model can be applied to estimate the vertical profile of flow speed (Maa et al., 2016). As u increases, bolstered vertical mixing will undermine vertical stratification, and our model can be effective in estimating total sediment transport in FGDSs.

5 Conclusions

With the assumptions that sediment transport is only driven by unstratified steady uniform currents and that bedload transport is negligible, a numerical model is set up to inspect the relationship between terms in the GEH formula on both sides of the equal sign, i.e. $C_D q_s^*$ and θ_b. Sediment transport regimes are differentiated according to differences in sediment transport behavior as indicated by calculation data. Between dune dominant and (mega-)ripple dominant regimes lies the coexistence zone, the regime shift in sediment transport, which is related to the degeneration of dune component in total bed roughness k_s, considerably reinforcing suspended sediment transport as the flow mobility parameter Ψ increases. Additionally, greater water depth h highlights such regime shift. Our study can be applied to future modeling of sediment transport and morphological evolution.

Code availability

The code used in this analysis is available as a Supplement.

© Author(s) 2018. CC BY 4.0 License.

Data availability

All data used in this analysis are available as a Supplement.

Author contribution

QY designed the study, TZ, QY and YW performed the research, TZ and QY wrote the paper, and SG supervised the research.

Competing interests

The authors declare that they have no conflict of interest.

Acknowledgments

The authors sincerely thank Prof. Zheng Bing Wang for his constructive comments on the original manuscript. This study was supported by the Natural Science Foundation of China (NSFC 41676081, 41676077) and the Fundamental Research Funds for the Central Universities (Grant No. 2016B00814).

References

Baas, J. H., Best, J. L., Peakall, J., and Wang, M.: A phase diagram for turbulent, transitional, and laminar clay suspension flows. Journal of Sedimentary Research, 79, 162-183. doi:10.2110/jsr.2009.025, 2009.

Blair, N. E. and Aller, R. C.: The fate of terrestrial organic carbon in the marine environment. Annual Review of Marine Science, 4, 401-423. doi:10.1146/annurev-marine-120709-142717, 2012.

Chien, N. and Wan, Z.: Mechanics of sediment transport. Reston, VA: ASCE Press. doi:10.1061/9780784404003, 1999.

Chien, N., Zhang, R., and Zhou, Z.: 河床演变学 [Fluvial processes]. Beijing, China: Science Press, 1987.

Engelund, F. and Hansen, E.: A monograph on sediment transport in alluvial streams. Copenhagen, Denmark: Teknisk Forlag. Retrieved from Delft University of Technology Library website: https://repository.tudelft.nl/islandora/object/uuid:81101b08-04b5-4082-9121-861949c336c9/, 1967.

Gao, S. and Collins, M. B.: Holocene sedimentary systems on continental shelves. Marine Geology, 352, 268-294. doi:10.1016/j.margeo.2014.03.021, 2014.

Earth Surf. Dynam. Discuss., https://doi.org/10.5194/esurf-2018-64
Manuscript under review for journal Earth Surf. Dynam.
Discussion started: 3 September 2018
© Author(s) 2018. CC BY 4.0 License.

Guy, H. P., Simons, D. B., and Richardson, E. V.: Summary of alluvial channel data from flume experiments, 1956-61 (Geological Survey Professional Paper 462-I). Washington, DC: Government Printing Office. Retrieved from USGS Publications Warehouse website: https://pubs.er.usgs.gov/publication/pp462I, 1966.

Julien, P. Y.: Erosion and Sedimentation (2nd ed.). New York City, NY: Cambridge University Press. doi:10.1017/CBO9780511806049, 2010.

Kuehl, S. A., Alexander, C. R., Blair, N. E., Harris, C. K., Marsaglia, K. M., Ogston, A. S., . . . Walsh, J. P.: A source-to-sink perspective of the Waipaoa River margin. Earth-Science Reviews, 153, 301-334. doi:10.1016/j.earscirev.2015.10.001, 2016.

Lapotre, M. G. A., Lamb, M. P., and McElroy, B.: What sets the size of current ripples? Geology, 45(3), 243-246. doi:10.1130/G38598.1, 2017.

Lee, H. J., Chu, Y. S., and Park, Y. A.: Sedimentary processes of fine-grained material and the effect of seawall construction in the Daeho macrotidal flat-nearshore area, northern west coast of Korea. Marine Geology, 157, 171-184. doi:10.1016/S0025-3227(98)00159-5, 1999.

Leithold, E. L., Blair, N. E., and Wegmann, K. W.: Source-to-sink sedimentary systems and global carbon burial: A river runs through it. Earth-Science Reviews, 153, 30-42. doi:10.1016/j.earscirev.2015.10.011, 2016.

Ma, H., Nittrouer, J. A., Naito, K., Fu. X., Zhang, Y., Moodie, A. J. Wang, Y., Wu, B., and Parker, G.: The exceptional sediment load of fine-grained dispersal systems: Example of the Yellow River, China. Science Advances, 3(5), e1603114. doi:10.1126/sciadv.1603114, 2017.

Maa, J.P., Shen, J., Shen, X., and Shao Y.: Vertical one-dimensional (1-D) simulations of horizontal velocity profiles (Special Scientific Report (Virginia Institute of Marine Science) No. 156). Gloucester Point, VA: Virginia Institute of Marine Science, College of William and Mary. doi:10.21220/V5RW2X, 2016.

Mangor, K., Drønen, N. K., Kærgaard, K. H., and Kristensen, S. E.: Shoreline Management Guidelines (4th ed.). Retrieved from DHI Free eBook website https://www.dhigroup.com/upload/campaigns/shoreline/assets/ShorelineManagementGuidelines_Feb2017-TOC.pdf, 2017

Manohar, M.: Mechanics of bottom sediment movement due to wave action (Technical Memorandum No. 75). Washington, DC: Beach Erosion Board, U.S. Army Corps of Engineers, 1955.

Molinas, A. and Wu, B.: Transport of sediment in large sand-bed rivers. Journal of Hydraulic Research, 39(2), 135-146. doi:10.1080/00221680109499814, 2001.

Nikuradse, J.: Strömungsgesetze in rauhen Rohren [Laws of flow in rough pipes]. Forschungsheft (Vol. 31). Berlin, Germany: Verein Deutscher Ingenieure, 1933.

Rodi, W. and Mansour, N. N.: Low Reynolds number k—ε modelling with the aid of direct simulation data. Journal of Fluid Mechanics, 250, 509-529. doi:10.1017/S0022112093001545, 1993.

© Author(s) 2018. CC BY 4.0 License.

Shields, A.: Anwendung der Aehnlichkeitsmechanik und der Turbulenzforschung auf die Geschiebebewegung [Application of similarity principles and turbulence research to bed-load movement] (Doctoral dissertation, Technical University Berlin, Berlin, Germany). Retrieved from Delft University of Technology Library website: https://repository.tudelft.nl/islandora/object/uuid:61a19716-a994-4942-9906-f680eb9952d6, 1936.

Soulsby, R. L.: Dynamics of marine sands: A manual for practical applications. Oxford, U.K.: Thomas Telford, 1997.

Soulsby, R. L. and Whitehouse, R. J. S.: Threshold of sediment motion in coastal environments. In: Pacific Coasts and Ports' 97: Proceedings of the 13th Australasian Coastal and Ocean Engineering Conference and the 6th Australasian Port and Harbour Conference (Vol. 1). Conference conducted at the meeting of Centre for Advanced Engineering, University of Canterbury, Christchurch, New Zealand, 1997.

van Maren, D. S., van Kessel, T., Cronin, K., and Sittoni, L.: The impact of channel deepening and dredging on estuarine sediment concentration. Continental Shelf Research, 95, 1-14. doi:10.1016/j.csr.2014.12.010, 2015.

van Rijn, L. C.: Principles of sediment transport in rivers, estuaries and coastal waters. Amsterdam, the Netherlands: Aqua Publications, 1993.

van Rijn, L. C.: Unified view of sediment transport by currents and waves. I: Initiation of motion, bed roughness, and bed-load transport. Journal of Hydraulic Engineering, 133(6), 649-667. doi:10.1061/(ASCE)0733-9429(2007)133:6(649), 2007a.

van Rijn, L. C.: Unified view of sediment transport by currents and waves. II: Suspended Transport. Journal of Hydraulic Engineering, 133(6), 668-689. doi:10.1061/(ASCE)0733-9429(2007)133:6(668), 2007b.

Venkatesan, M. I., Merino, O., Baek, J., Northrup, T., Sheng, Y., and Shisko, J.: Trace organic contaminants and their sources in surface sediments of Santa Monica Bay, California, USA. Marine Environmental Research, 69, 350-362. doi:10.1016/j.marenvres.2009.12.010, 2010.

Wang, Y. P., Gao, S., Jia, J., Thompson, C. E. L., Gao, J., and Yang, Y.: Sediment transport over an accretional intertidal flat with influences of reclamation, Jiangsu coast, China. Marine Geology, 291-294, 147-161. doi:10.1016/j.margeo.2011.01.004, 2012.

Winterwerp, J. C.: Reducing Harbor Siltation. I: Methodology. Journal of Waterway, Port, Coastal, and Ocean Engineering, 131(6), 258-266. doi:10.1061/(ASCE)0733-950X(2005)131:6(258), 2005.

Wright, L. D.: Morphodynamics of Inner Continental Shelves. Boca Raton, FL: CRC Press, 1995.

Wright, L. D. and Nittrouer, C. A.: Dispersal of River Sediments in Coastal Seas: Six Contrasting Cases. Estuaries, 18(3), 494-508. doi:10.2307/1352367, 1995.

© Author(s) 2018. CC BY 4.0 License.

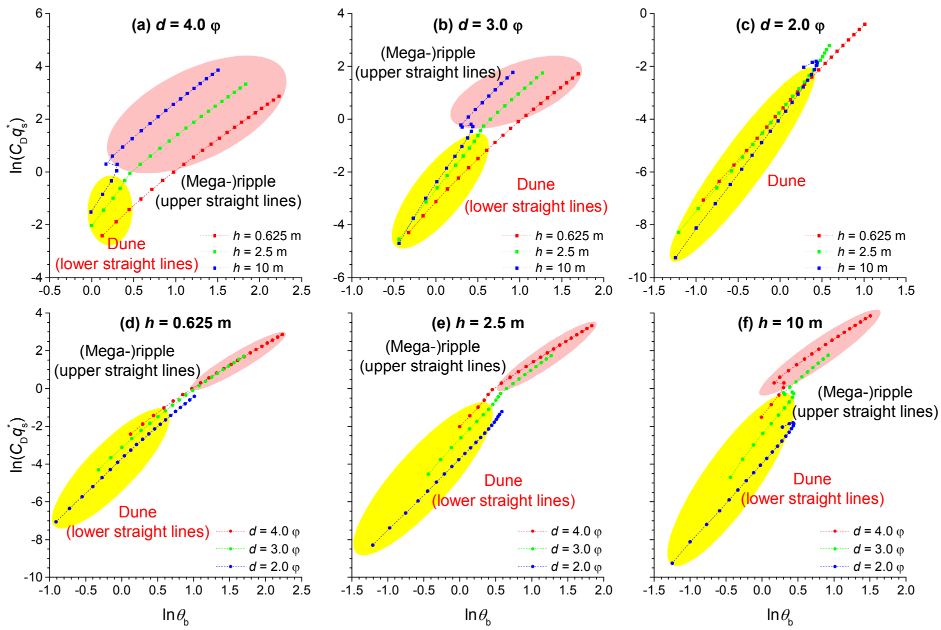

Figure 1: Log-log plotted relationships between y-axis: product ($C_{\mathrm{D}}q_{\mathrm{s}}^{*}$) of total bed drag coefficient ($C_{\mathrm{D}} = \left[\frac{0.4}{1+\ln\left(\frac{k_s}{30h}\right)}\right]^2$) and dimensionless sediment transport rate ($q_{\mathrm{s}}^{*} = \frac{q_{\mathrm{s}}}{\rho_{\mathrm{s}}\sqrt{(s-1)gd^3}}$, i.e. Einstein number), and x-axis: dimensionless bed shear stress ($\theta_{\mathrm{b}} = \frac{\tau_{\mathrm{b}}}{(\rho_{\mathrm{s}}-\rho)gd}$, i.e. Shields number), given specific combinations of typical bed sediment grain size (d = 4.0, 3.0, 2.0 φ) and water depth (h = 0.625, 2.5, 10 m) under fluvial, coastal, and flume settings. Data points are categorized into dune dominant (lower straight lines) and (mega-)ripple dominant (upper straight lines, associated with typical sediment transport behavior in FGDSs) regimes, and the coexistence (in-between shifts) zone, according to how the sediment transport behavior ($C_{\mathrm{D}}q_{\mathrm{s}}^{*}$) responds to the fluid flow (θ_{b}) through the bed. Bed sediment grain size fixed, the two regimes diverge as water depth increases (a~c). The (mega-)ripple regime tend to vanish with respect to a coarser bed, regardless of the current water depth (d~f).

Earth Surf. Dynam. Discuss., https://doi.org/10.5194/esurf-2018-64
Manuscript under review for journal Earth Surf. Dynam.
Discussion started: 3 September 2018
© Author(s) 2018. CC BY 4.0 License.

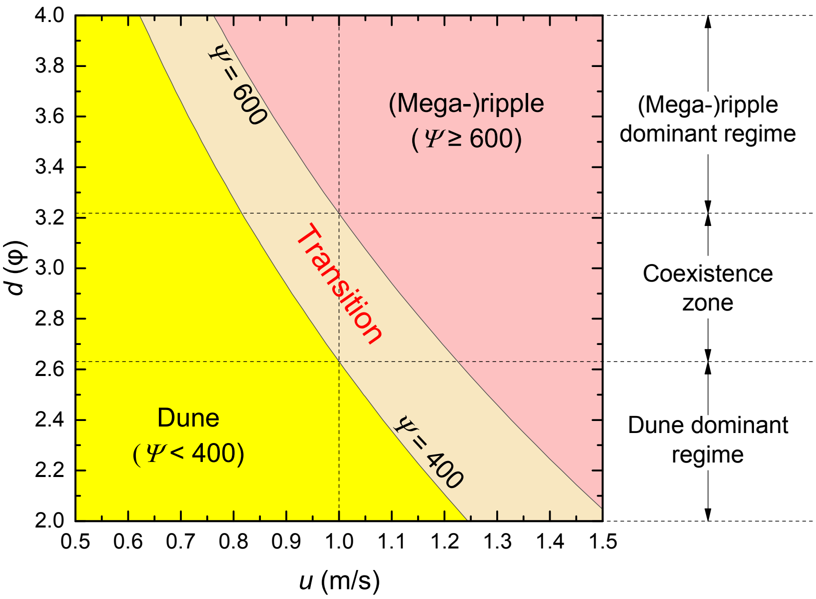

Figure 2: Bedform category as a function of flow mobility parameter ($\Psi = \frac{u^2}{(s-1)gd}$). Data points with specific Ψ values are classified as dune ($\Psi < 400$), transition ($400 \leq \Psi < 600$), and (mega-)ripple ($\Psi \geq 600$) regions. For typical vertical-averaged flow speed values ($u \in [0.5, 1.5]$ (m/s)) in fluvial and coastal areas, sediment transport over a particular grain-sized bed falls into: either a dominant regime (for (mega-)ripple dominant regime, d = 3.22 ~ 4.0 φ; for dune dominant regime, d = 2.0 ~ 2.63 φ), as long as the contribution of corresponding bedform data points exceeds 50%; or the coexistence zone (d = 2.63 ~ 3.22 φ), when both dune and (mega-)ripple points fail to become predominant (>50%).

© Author(s) 2018. CC BY 4.0 License.

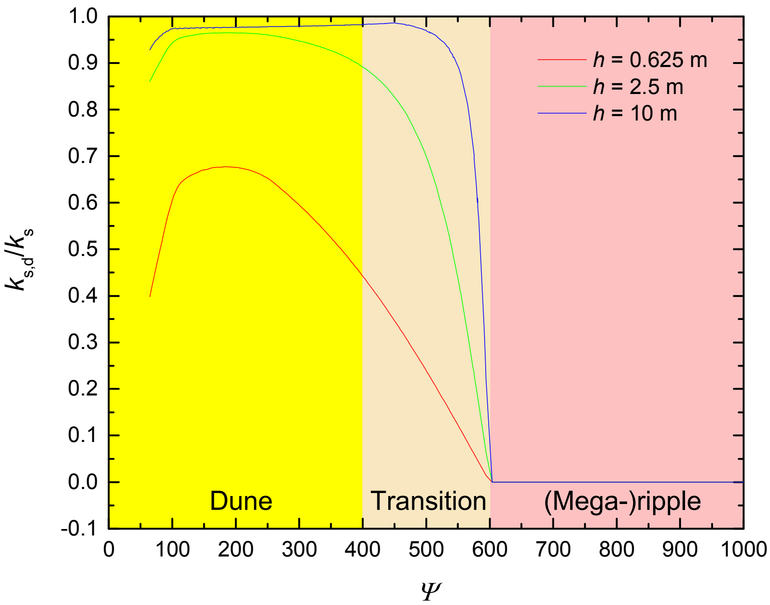

Figure 3: Changes in the weight ($k_{s,d}/k_s$) of dune component ($k_{s,d}$) in total bed roughness height (k_s), as a function of flow mobility parameter ($\Psi = \frac{u^2}{(s-1)gd}$). Bedform categories are marked as they are in Figure 2. Under a specific water depth, the ratio $k_{s,d}/k_s$ experiences a sharp increase to reach a high stage in the dune region, then it declines hugely to 0 in the narrow transition zone, witnessing a bedform shift. As determined by the van Rijn (2007) method, this ratio remains zero in the (mega-)ripple region, indicating no dune formation above the bed. Aside from its variation with Ψ, the upper limit of this ratio increases rapidly as water depth goes up, exceeding 0.95 once the water depth is greater than 2.5 m.

© Author(s) 2018. CC BY 4.0 License.

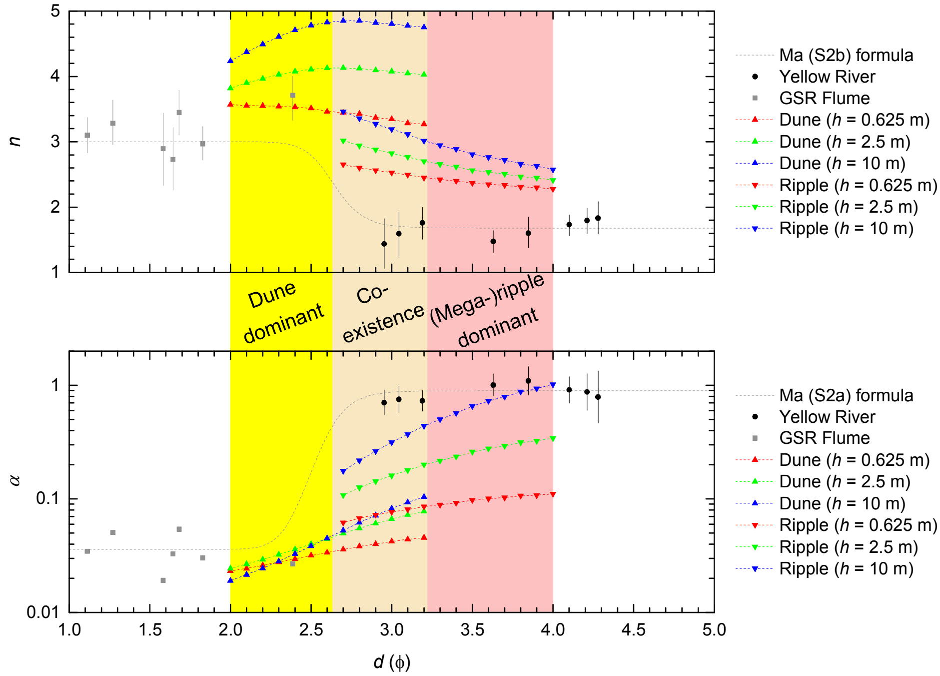

Figure 4: Changes of y-axes: exponent (n) and coefficient (α) of dimensionless bed shear stress ($\theta_{\mathrm{b}} = \frac{\rho C_{\mathrm{D}} u^2}{(s-1)\rho g d}$, i.e. Shields number) in the Generalized Engelund-Hansen (GEH) formula ($C_{\mathrm{D}} q_{\mathrm{s}}^{*} = \alpha \theta_{\mathrm{b}}^{\mathrm{n}}$), with respect to x-axis: bed sediment grain size (d). Bed regimes with respect to bed sediment grain size are marked as what they are in Figure 2. As water depth (h) increases, data plots see increases in average n (dune - 3.5 ~ 4.6, (mega-)ripple - 2.3 ~ 2.8) and (mega-)ripple α (0.10 ~ 0.76), while average dune α (0.028 ~ 0.033) varies little. If relating dune and (mega-)ripple points of a specific water depth, the joint curves (n-d and α-d) (1) show similar trends (almost Logistic, and the regime shift/transition in the coexistence zone), as shown in Ma et al. (2017) where Logistic functions are derived out of Yellow River and Guy-Simons-Richardson (1966) flume data; (2) travel upwards and diverge as the water depth increases, representing a more crucial role that fluid flow (θ_{b}) plays in shaping the sediment transport behavior ($C_{\mathrm{D}} q_{\mathrm{s}}^{*}$).